

# Tensor renormalization of quantum many-body systems using projected entangled simplex states

Z. Y. Xie<sup>1\*</sup>, J. Chen<sup>1\*</sup>, J. F. Yu<sup>1</sup>, X. Kong<sup>1</sup>, B. Normand<sup>2</sup>, and T. Xiang<sup>1</sup>

<sup>1</sup>*Institute of Physics, Chinese Academy of Sciences, P.O. Box 603, Beijing 100190, China and*

<sup>2</sup>*Department of Physics, Renmin University of China, Beijing 100872, China*

We propose a new class of tensor-network states, which we name projected entangled simplex states (PESS), for studying the ground-state properties of quantum lattice models. These states extend the pair-correlation basis of projected entangled pair states (PEPS) to a simplex. PESS are an exact representation of the simplex solid states and provide an efficient trial wave function that satisfies the area law of entanglement entropy. We introduce a simple update method for evaluating the PESS wave function based on imaginary-time evolution and the higher-order singular-value decomposition of tensors. By applying this method to the spin-1/2 antiferromagnetic Heisenberg model on the kagome lattice, we obtain accurate and systematic results for the ground-state energy, which approach the lowest upper bounds yet estimated for this quantity.

PACS numbers: 64.60.Cn, 05.50.+q, 75.10.Hk, 64.60.F-

## I. INTRODUCTION

The theory of tensor-network states is evolving rapidly into an interdisciplinary field involving condensed matter physics, quantum information theory, renormalization group theory, and even quantum gravity. From its initial proposals [1–3], through the development of representations and techniques [4–12], it has become increasingly popular in the simulation of both classical models [3, 7, 11, 13] and strongly correlated quantum systems [8–10, 14–16], providing deep insight into the physical properties of quantum many-body states. In one dimension, the tensor-network state is known as a matrix-product state (MPS) [17], and is also the wave function generated by the density matrix renormalization group (DMRG) algorithm [18]. A MPS may be viewed as a trial wave function arising from virtual entangled pairs formed between two nearest-neighbor sites of a lattice. Thus it yields a local description of quantum many-body states based on their entanglement structure. A typical example of a MPS is the  $S = 1$  Affleck-Kennedy-Lieb-Tasaki (AKLT) state [19], which provides a prototype framework for understanding the physics of the Haldane excitation gap in integer quantum spin chains.

Projected entangled pair states (PEPS) constitute a natural generalization of MPS to two and higher dimensions [4]. This generalization, motivated by two-dimensional AKLT states [19], is obtained by distributing virtual maximally entangled states between any two nearest-neighbor sites. It leads to a faithful representation of the many-body wave function of the ground state. Crucially, PEPS capture the boundary area law obeyed by the entanglement entropy, which is believed to be the most important ingredient causing quantum systems to behave differently from classical ones [20].

It is precisely the existence of entanglement that is responsible for such exotic phenomena as quantum phase transitions and topological quantum order. Furthermore, PEPS allow a many-body ground-state wave function, which contains exponentially many degrees of freedom, to be calculated approximately but accurately on a polynomial time scale. In particular, for a translationally invariant system, the understanding of the whole wave function can be mapped to the problem of studying the properties of just a single, or a small number of, local tensor(s).

Despite its strengths, the PEPS representation has two significant disadvantages. It describes correctly the entanglement of adjacent basis states, making it a good representation of AKLT-type states, and in principle it can be used to represent all quantum states satisfying the area law of entanglement. However, in practical calculations, the bond dimension must be kept as small as possible to obtain sufficient accuracy and efficiency, and this means that PEPS may not always provide a good representation for the quantum states of some systems. As an example, applying the PEPS algorithm on a triangular lattice is technically difficult due to the high coordination number. A local tensor in PEPS on a triangular lattice contains seven indices, six from the virtual bond degrees of freedom and one from the physical degrees of freedom. Because the size of each tensor scales as  $D^6$ , the bond dimension  $D$  that can be handled practically by current techniques is limited to a very small value (approximately 2–5).

The other disadvantage of PEPS concerns their application to frustrated systems. They have been used to provide a very good variational ansatz for the ground-state wave function of two-dimensional quantum spin models on the square and honeycomb lattices [8–10]. However, for the antiferromagnetic Heisenberg model on the kagome lattice, we found that the entanglement spectra of the local tensors for each one of the four bonding directions are always doubly degenerate, due to the frustrated lattice geometry, when  $D > 3$ . This causes a numerical

---

\*The first two authors contributed equally to this work.

instability that is difficult to correct in the calculation of expectation values, and in this case the PEPS ground-state energy does not converge with increasing  $D$ . More generally, and as we discuss in detail below, it is difficult to use PEPS to represent a quantum state in which the local correlation or entanglement among all the basis states within a cluster (or simplex) containing more than two lattice sites, for example the simplex solid state proposed by Arovas [21], becomes important.

In this work, we solve these problems by introducing a new class of tensor-network states. We call these Projected Entangled Simplex States (PESS), because they can be understood in terms of entangled simplex states of virtual systems that are locally projected onto the physical basis states. This class of states arises naturally as the exact representation of the simplex solid states, but is of much broader use because, similar to PEPS, any state can be represented by PESS if the virtual dimension is sufficiently large. PESS extend pair correlations to simplex correlations and hence constitute a natural generalization of the PEPS representation.

By the word “simplex” we refer to a cluster of lattice sites, which constitute the basic unit, or “building block,” of a two- or higher-dimensional lattice. As an example, a triangle is a building block of the kagome lattice (Fig. 1) and can be taken as a simplex for this lattice. However, one may also combine a number of simplices to form a larger simplex; the choice of a simplex is not unique, but it should reflect correctly the symmetry of the system. If a simplex contains  $N$  lattice sites, we refer to the corresponding PESS as an  $N$ -PESS. If we release the definition of the simplex and allow it to contain just two neighboring sites,  $N = 2$ , the PESS are precisely the PEPS. Thus PESS include PEPS as a subclass. As for PEPS, PESS are defined by introducing a number of virtual basis states at each node of the lattice. In addition to the local tensors, defined similarly to the PEPS framework for projecting out the physical states from the virtual basis states at each node, the PESS contain a new type of local tensor, which we call the “entangled simplex tensor.” This tensor describes the correlation, or entanglement, of virtual particles within the full simplex, and it is this feature that addresses the frustration problem. An  $N$ -PESS with  $N \geq 3$  is constructed as a tensor-network product of these two types of local tensor. Examples of this process are presented in Sec. II.

Concerning the bond-dimension problem of PEPS, we provide a brief example using the kagome lattice. The order (number of tensor indices) of the local tensors in a PEPS representation is five and the size of the local tensor is  $dD^4$ , where  $d$  is the dimension of the physical basis states. For PESS, as we will illustrate in Sec. II, both types of local tensors have only three indices, their sizes being  $dD^2$  for the regular projection tensors and  $D^3$  for the entangled simplex tensor. Thus in practical calculations a significantly larger bond dimension may be studied in the PESS representation than by PEPS. While this is a major advantage of PESS, it does not

mean a PESS representation is always more efficient than a PEPS one. For AKLT states, PEPS remain the most efficient representation, whereas for simplex solid states, PESS are undoubtedly the most efficient.

We close this introduction by noting that general insight into the structure of a quantum wave function may be obtained from singular value decomposition (SVD). In the DMRG procedure in one spatial dimension, Schmidt decomposition of the wave function is a SVD, and the SVD spectrum is simply the square root of the eigenvalues of the reduced density matrix. Indeed, at the formal level any wave function generated by DMRG can be expressed as a projected “maximally entangled pair” state; in this sense, the PEPS description is equivalent to a SVD and the physical content of a MPS or PEPS ansatz can be understood more generally from the entanglement structure of the wave function under SVD. However, the PEPS approach offers a means of constructing the wave function using only the local entanglement structure, which greatly simplifies the construction of the PESS representation in comparison with a SVD approach. This said, SVD [8–10] and higher-order SVD (HOSVD) [11] of tensors is fundamental in constructing renormalization schemes for tensor-network representations of systems in dimensions higher than one, and is the core of the methods employed in Sec. IV.

This paper is arranged as follows. In Sec. II, in order to elaborate the physics underlying the PESS, we introduce an  $SU(2)$  simplex solid state of spin  $S = 2$  and construct explicitly both its PESS representation and the parent Hamiltonian. In Sec. III we propose the PESS as a trial wavefunction for the ground states of quantum lattice models. We introduce in Sec. IV a simple update approach for evaluating the PESS wavefunction based on the HOSVD of tensors. By applying this approach to the spin-1/2 Heisenberg model on the kagome lattice, we obtain the ground-state energy as a function of the bond dimension  $D$  for simplices with  $N = 3, 5$ , and  $9$ . Section V contains a summary and discussion.

## II. PESS REPRESENTATION OF SIMPLEX SOLID STATES

The simplex solid state of  $SU(N)$  quantum antiferromagnets was introduced by Arovas [21]. It extends the bond singlets of the AKLT state to  $S = 0$  states of  $N$ -site simplices, with  $N \geq 3$ . Each simplex accommodates a virtual quantum singlet. As with the AKLT states, the simplex solid states are extinguished by certain local projection operators. This feature allows one to construct a many-body Hamiltonian for which the simplex solid state is an exact ground state, usually with a gap to all low-energy excitations.

The wave function of simplex solid states can be expressed as a tensor-network state. This tensor-network state is the PESS, a result we illustrate by constructing a simplex solid state and its PESS representation for

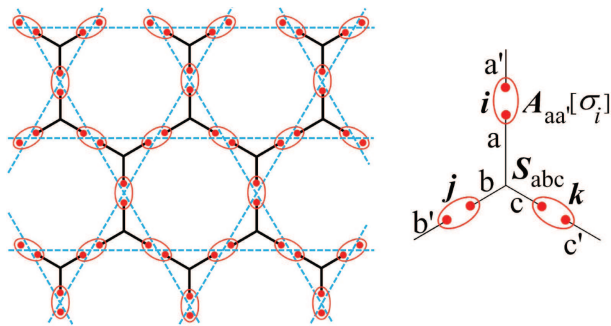


FIG. 1: (Color online) The spin-2 simplex solid state on the kagome lattice (blue dashed lines). The entangled simplex tensors  $S$  form a honeycomb lattice (black solid lines) and the projection tensors  $A$  are defined on the decorating sites of this honeycomb lattice.

the  $S = 2$  Heisenberg model on the kagome lattice. The kagome geometry is a two-dimensional network of corner-sharing triangles, each forming a three-site simplex. As shown in Fig. 1, the simplices form a honeycomb lattice, on which the kagome lattice is formed by the decorating sites.

### A. Spin-2 kagome lattice

A physical  $S = 2$  state can be regarded as a symmetric superposition of two virtual  $S = 1$  spins. On the kagome lattice, two neighboring triangles (simplices) share a single site. As in an AKLT state, we can assign each of the  $S = 1$  spins to one of the simplices associated with this site. There are then three  $S = 1$  spins on each simplex triangle, and their product contains a unique spin singlet state,

$$\underline{1} \otimes \underline{1} \otimes \underline{1} = \underline{0} \oplus (3 \times \underline{1}) \oplus (2 \times \underline{2}) \oplus \underline{3}. \quad (1)$$

This allows us to define a virtual singlet on the simplex,

$$|0, 0\rangle = \frac{1}{\sqrt{6}} \sum_{s_i s_j s_k} \varepsilon_{s_i s_j s_k} |s_i\rangle |s_j\rangle |s_k\rangle, \quad (2)$$

where  $|s_i\rangle$  ( $s_i = -1, 0, 1$ ) is a basis state of the  $S = 1$  spin at site  $i$  and  $\varepsilon_{ijk}$  is the Levi-Civita antisymmetric tensor.

The many-body state with this singlet on each simplex is a simplex solid state. Its wavefunction, illustrated in Fig. 1, is a PESS, which can be expressed as

$$|\Psi\rangle = \text{Tr}(\dots S_{abc} A_{aa'}[\sigma_i] A_{bb'}[\sigma_j] A_{cc'}[\sigma_k] \dots) |\dots \sigma_i \sigma_j \sigma_k \dots\rangle, \quad (3)$$

where the trace is over all spin configurations and all bond indices.  $S_{abc}$  is the entangled simplex tensor defined on the simplex honeycomb lattice. The physical basis states  $\{\sigma_i, \sigma_j, \dots\}$  are defined on the decorating sites of the honeycomb lattice  $\{i, j, \dots\}$  (i.e. on the kagome lattice

sites). The Roman letters  $\{a, b, \dots\}$  denote the virtual bond states. Because the virtual spins in each simplex triangle form a spin singlet,  $S_{ijk}$  in this case is simply an antisymmetric Levi-Civita tensor,

$$S_{ijk} = \varepsilon_{ijk}.$$

$A_{i,i'}[\sigma_1]$  is a  $3 \times 3$  matrix, which maps two virtual  $S = 1$  spins onto an  $S = 2$  physical spin, and whose components are given by the Clebsch-Gordan coefficients of the  $SU(2)$  Lie algebra,

$$A_{11}[2] = A_{33}[-2] = 1,$$

$$A_{12}[1] = A_{21}[1] = A_{23}[-1] = A_{32}[-1] = \frac{1}{\sqrt{2}},$$

$$A_{13}[0] = A_{31}[0] = \frac{1}{\sqrt{6}},$$

$$A_{22}[0] = \frac{2}{\sqrt{6}},$$

while all other matrix elements are zero.

For this  $S = 2$  PESS representation, the total spins have the following possibilities on any given bond of the kagome lattice,

$$\underline{2} \otimes \underline{2} = \underline{0} \oplus \underline{1} \oplus \underline{2} \oplus \underline{3} \oplus \underline{4}. \quad (4)$$

The fact that each bond belongs to a simplex means that it cannot be in the fully symmetric  $S = 4$  state. Thus this PESS is an exact ground state of the Hamiltonian

$$H = \sum_{\langle ij \rangle} P_4(ij), \quad (5)$$

where  $P_4(ij)$  is a projection operator projecting the spin states on any nearest-neighbor bond  $\langle ij \rangle$  onto a state with total spin  $S = 4$ .  $P_4(ij)$  can be expressed using the local spin operators as

$$P_4(ij) = -\frac{1}{280}T_{ij} + \frac{3}{1120}T_{ij}^2 - \frac{1}{2016}T_{ij}^3 + \frac{1}{40320}T_{ij}^4,$$

TABLE I: Coefficients for projection operators in Eq. (7).

$n$	$P_{4,n}$	$P_{5,n}$	$P_{6,n}$
1	$-\frac{9}{440}$	$\frac{1}{360}$	$-\frac{1}{5544}$
2	$\frac{1017}{61600}$	$-\frac{173}{75600}$	$\frac{5}{33264}$
3	$-\frac{23}{6160}$	$\frac{197}{362880}$	$-\frac{731}{19958400}$
4	$\frac{39}{123200}$	$-\frac{547}{10886400}$	$\frac{61}{17107200}$
5	$-\frac{23}{2217600}$	$\frac{41}{21772800}$	$-\frac{1}{6842880}$
6	$\frac{1}{8870400}$	$-\frac{1}{43545600}$	$\frac{1}{479001600}$

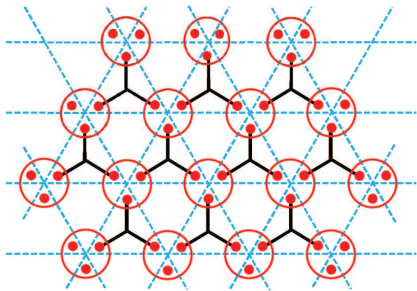


FIG. 2: (Color online) Schematic representation of the simplex solid state on the triangular lattice (blue dashed lines).

where  $T_{ij} = (\mathbf{S}_i + \mathbf{S}_j)^2$ . We note here that the spin-2 AKLT state on the kagome lattice is also the ground state of this Hamiltonian. In fact, it can be shown that the PESS wave function for this system, defined by Eq. (3), is identical to the AKLT state [22]. This is a very special property of the case we have chosen for illustration; in the general case, there is no AKLT-type representation for most simplex solid states.

In the PESS of Fig. 1, half of the virtual spins at the three vertices on any given simplex are quenched to zero. Thus the total spin on a simplex cannot exceed  $S = 3$ . If we allow the system to have three-site interactions within each simplex, then it is straightforward to show that the above PESS is also the ground state of the Hamiltonian

$$H = \sum_{\alpha} (J_4 P_{\alpha,4} + J_5 P_{\alpha,5} + J_6 P_{\alpha,6}), \quad (6)$$

where  $\alpha$  represents a simplex triangle,  $J_4$ ,  $J_5$ , and  $J_6$  are non-negative coupling constants, and  $P_{\alpha,S}$  is the operator projecting a state at each simplex triangle onto a state with total spin  $S$ . Using the spin operators on the three vertices of the simplex,  $(\mathbf{S}_{\alpha,1}, \mathbf{S}_{\alpha,2}, \mathbf{S}_{\alpha,3})$ ,  $P_{\alpha,S}$  can be expressed as

$$P_{\alpha,S} = \sum_{n=1}^6 P_{S,n} (\mathbf{S}_{\alpha,1} + \mathbf{S}_{\alpha,2} + \mathbf{S}_{\alpha,3})^{2n} \quad (7)$$

where the coefficients  $P_{S,n}$  are given in Table I.

### B. Generalizations to different spins and lattice geometries

The preceding discussion for the  $S = 2$  simplex solid state can be extended to systems of any higher spin, provided that a unique spin singlet can be formed by the virtual spins in each simplex [21]. We continue our illustration of the PESS representation by discussing briefly its further generalization to describe simplex solids on different lattices, choosing as examples the triangular (Fig. 2) and square (Fig. 3) geometries.

For the simplex solid state on the triangular lattice shown in Fig. 2, the physical spin is formed by three vir-

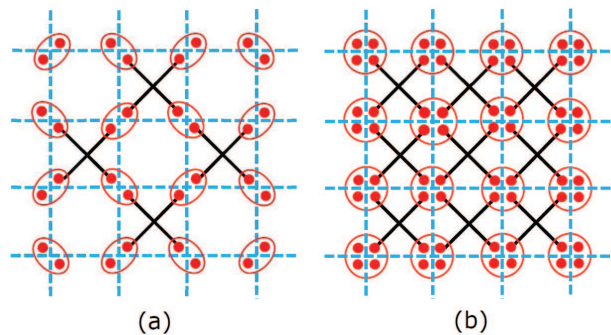


FIG. 3: (Color online) Schematic representation of two types of simplex solid state on the square lattice (blue dashed lines).

tual spins. The simplex solid state is defined on a honeycomb lattice, which is bipartite, with the simplex tensors on one of the sublattices and the projection tensors on the other. If one assumes the virtual spin is still in the spin-1 representation, then the physical spin will be in an  $S = 3$  state. The simplex tensor is a  $D = 3$  antisymmetric Levi-Civita tensor, as for the kagome lattice. The projection tensor is now a four-indexed quantity, with three virtual indices and one physical index. It maps three virtual  $S = 1$  states onto a fully symmetric  $S = 3$  physical state. The parent Hamiltonian for this PESS representation can be constructed in the same way as for the kagome lattice. A parent Hamiltonian containing only nearest-neighbor interaction terms is given by

$$H = \sum_{\langle ij \rangle} P_6(ij), \quad (8)$$

where  $P_6(ij)$  is the projection operator mapping the two  $S = 3$  states onto a state with total spin  $S = 6$ .

The definition of simplex solid states depends on the choice of simplex, and on a given lattice is not unique. As an example of this, we show in Fig. 3 that two kinds of simplex solid state can be defined on the square lattice. If the lattice is taken as an edge-sharing simplex lattice [Fig. 3(b)], there are four virtual particles on each lattice site and the simplex solid state so defined is translationally invariant. The site projection is a five-indexed tensor. If instead we take the square lattice as a vertex-sharing simplex lattice [Fig. 3(a)], then each site contains only two virtual particles and the site projection is a three-indexed tensor. The order of the projection tensors is also lower than the edge-sharing case. While this simplex solid state is also translationally invariant, the lattice unit cell is doubled.

The simplex solid state can also be considered in systems where the generalized “spin” at each site has  $SU(N)$  symmetry, or obeys any other Lie algebra. A general discussion of the  $SU(N)$  simplex solid states is given in Ref. [21]. There is always a PESS representation of simplex solid states and it is readily constructed from the Clebsch-Gordon coefficients, or more generally from the



decomposition rules of the irreducible representations.

### III. PESS AS A VARIATIONAL ANSATZ

As for PEPS, it can be shown that PESS provide a good approximation for the ground-state wave function, which satisfies the entanglement area law. Thus PESS can be also regarded as a trial wave function for the ground state of a quantum lattice model. To understand this statement clearly, we take for illustration the spin-1/2 Heisenberg antiferromagnet on the kagome lattice and demonstrate how to generate a PESS wavefunction by imaginary-time evolution.

The Heisenberg model is defined on any lattice by

$$H = J \sum_{\langle ij \rangle} (S_i^x S_j^x + S_i^y S_j^y + S_i^z S_j^z), \quad (9)$$

where we take the simplest version in which  $\langle ij \rangle$  denotes the summation only over all nearest neighbors. To perform the imaginary-time evolution, we divide this Hamiltonian into a sum of three terms,

$$H = H_x + H_y + H_z, \quad (10)$$

where

$$H_\alpha = J \sum_{\langle ij \rangle} S_i^\alpha S_j^\alpha \quad (11)$$

with  $\alpha = x, y, z$ . All terms within  $H_\alpha$  commute, but  $H_x$ ,  $H_y$ , and  $H_z$  do not commute with each other. To evaluate the partition function, we use the Trotter-Suzuki formula to decompose the evolution operator  $e^{-\tau H}$  into a product of three terms,

$$e^{-\tau H} = e^{-\tau H_x} e^{-\tau H_y} e^{-\tau H_z} + \mathcal{O}(\tau^2) \quad (12)$$

for small  $\tau$ . In this approximation, the partition function can be expressed as

$$\begin{aligned} Z &= \text{Tr} e^{-\beta H} \approx \text{Tr} (e^{-\tau H})^M \\ &\approx \text{Tr} (e^{-\tau H_x} e^{-\tau H_y} e^{-\tau H_z})^M, \end{aligned} \quad (13)$$

where  $\beta = M\tau$ .

We define a set of basis states specific to the spin-1/2 case,

$$|\sigma_j^{\alpha,n}\rangle = \{|\sigma_j^{\alpha,n}\rangle; j = 1, \dots, L\}, \quad (14)$$

where  $|\sigma_j^{\alpha,0}\rangle = |\sigma_j^{\alpha,M}\rangle$  and  $L$  is the total number of lattice sites. Here  $|\sigma_j^{\alpha,n}\rangle$  is the local basis state of  $S_j^\alpha$ ,

$$S_j^\alpha |\sigma_j^{\alpha,n}\rangle = \sigma_j^{\alpha,n} |\sigma_j^{\alpha,n}\rangle, \quad (15)$$

with eigenvalue  $\sigma_j^{\alpha,n} = \pm 1$ . By inserting these basis sets into Eq. (13), we express the partition function in the

form

$$\begin{aligned} Z &\approx \sum_{\{\sigma^x, \sigma^y, \sigma^z\}} \prod_{n=1}^M \langle \sigma^{x,n} | e^{-\tau H_x} | \sigma^{x,n} \rangle \langle \sigma^{x,n} | \sigma^{y,n} \rangle \\ &\quad \times \langle \sigma^{y,n} | e^{-\tau H_y} | \sigma^{y,n} \rangle \langle \sigma^{y,n} | \sigma^{z,n} \rangle \\ &\quad \times \langle \sigma^{z,n} | e^{-\tau H_z} | \sigma^{z,n} \rangle \langle \sigma^{z,n} | \sigma^{x,n-1} \rangle. \end{aligned} \quad (16)$$

The basis sets  $|\sigma^{y,n}\rangle$  and  $|\sigma^{x,n}\rangle$  are connected by the transformation matrix  $\langle \sigma^{x,n} | \sigma^{y,n} \rangle$ , which is a product of local transformation matrices at each site,

$$A_{\sigma^{x,n}, \sigma^{y,n}}^x = \langle \sigma^{x,n} | \sigma^{y,n} \rangle = \prod_j A_{j, \sigma^{x,n}, \sigma^{y,n}}^x, \quad (17)$$

$$A_j^x = \frac{1}{2} \begin{pmatrix} 1+i & 1-i \\ 1-i & 1+i \end{pmatrix}. \quad (18)$$

Similarly, one obtains for the other matrices

$$A_{\sigma^{y,n}, \sigma^{z,n}}^y = \prod_j A_{j, \sigma^{y,n}, \sigma^{z,n}}^y, \quad (19)$$

$$A_j^y = \frac{1}{\sqrt{2}} \begin{pmatrix} 1 & -i \\ 1 & i \end{pmatrix} \quad (20)$$

and

$$A_{\sigma^{z,n}, \sigma^{x,n-1}}^z = \prod_j A_{j, \sigma^{z,n}, \sigma^{x,n-1}}^z, \quad (21)$$

$$A_j^z = \frac{1}{\sqrt{2}} \begin{pmatrix} 1 & 1 \\ 1 & -1 \end{pmatrix}. \quad (22)$$

In Eq. (16),  $\langle \sigma^{\alpha,n} | e^{-\tau H_\alpha} | \sigma^{\alpha,n} \rangle$  is the matrix element of the classical Ising model  $H_\alpha$ , which is also the Boltzmann weight of  $H_\alpha$  for a given basis set  $|\sigma^{\alpha,n}\rangle$ . As discussed in Ref. [10], this quantity can be written as a product of local tensors,

$$\langle \sigma^{\alpha,n} | e^{-\tau H_\alpha} | \sigma^{\alpha,n} \rangle = \prod_{\nabla_{ijk}} S_{\sigma_i^{\alpha,n}, \sigma_j^{\alpha,n}, \sigma_k^{\alpha,n}}^{\alpha}, \quad (23)$$

with

$$S_{\sigma_i, \sigma_j, \sigma_k}^\alpha = \exp[-\tau J (\sigma_i \sigma_j + \sigma_k \sigma_i + \sigma_j \sigma_k)].$$

It is at this point where the lattice geometry enters, the symbol  $\nabla$  indicating that the product is taken over all simplices (triangles) of the kagome lattice.

Now the partition function becomes

$$Z \approx \text{Tr} T^M, \quad (24)$$

where  $T = T^x T^y T^z$  is the tensor evolution operator and the matrix elements of  $T^\alpha$ , given by

$$\langle \sigma' | T^\alpha | \sigma \rangle = \prod_{\nabla_{ijk}} S_{\sigma'_i, \sigma'_j, \sigma'_k}^\alpha \prod_j A_{\sigma'_j, \sigma_j}^j, \quad (25)$$

contain both the entangled simplex and projection tensors.  $T^\alpha$  defines a simplex tensor network operator on the

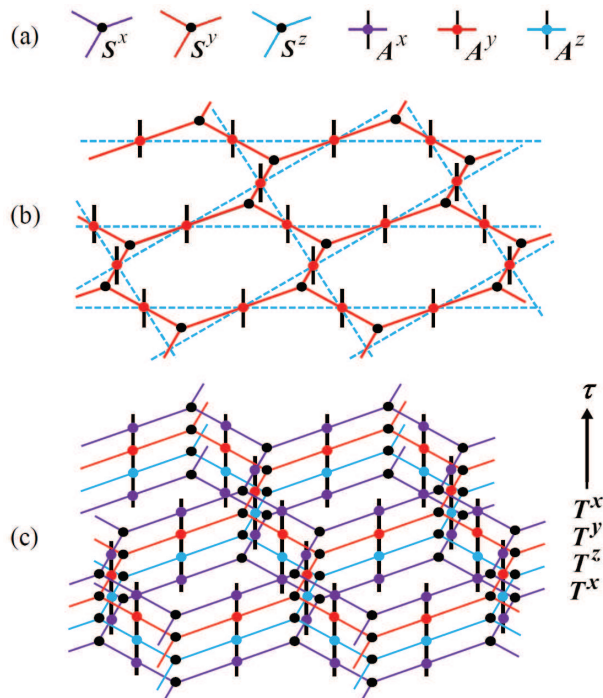


FIG. 4: (Color online) Graphical representation of simplex tensor operators on the kagome lattice. (a) Simplex ( $S$ ) and projection ( $A$ ) operators. (b) Tensor  $T^z$  specified in Eq. (25). (c) One evolution step of the simplex tensor operator  $T = T^x T^y T^z$  describing the partition function (16).

decorated honeycomb lattice, a graphical representation of which is shown in Fig. 4. Thus the partition function is expressed as a product of simplex tensor network operators.

In the limit of zero temperature,  $\beta \rightarrow \infty$ , the partition function (or the density matrix) is determined purely by the largest eigenvalue and eigenvector of the evolution operator  $T$ . The largest eigenvector may be found by the power method, starting from an arbitrary initial wavefunction  $|\Psi_0\rangle$ , which is not orthogonal to this eigenvector. Due to the simplex network structure of the evolution operators  $T^\alpha$ , it is natural to assume that  $|\Psi_0\rangle$  is a PESS wave function. When  $T$  is applied to  $|\Psi_0\rangle$ , its PESS structure is retained, and thus the ground-state wave function can indeed be expressed using PESS. Of course, at each projection, or application of  $T^\alpha$  to the wave function, the bond dimension of the PESS is doubled. Thus in real calculations the bond dimension must be truncated to find an approximate PESS solution for the ground-state wave function.

#### IV. SIMPLE UPDATE METHOD FOR PESS CALCULATIONS

In principle, the PESS wave function can be determined by using the variational approaches developed for

PEPS. However, the bond dimensions of PESS that can be treated with these techniques are generally very small. An approximate but efficient means of determining the PEPS wave function is the “simple update” method first proposed by Jiang *et al.* [8], which is in essence an entanglement mean-field approach. It avoids a full calculation of the tensor environment during the step where the wave function is updated by imaginary-time evolution, which is usually the rate-limiting step in the calculation. This procedure converts a global minimization problem into a local one, yielding a fast algorithm that allows us to reach large values of the bond dimension  $D$ . It is more effective for gapped systems and is almost exact on Bethe lattices [6, 16] (a one-dimensional chain can be regarded as the simplest Bethe lattice). However, the accuracy of the results falls substantially when the system is close to a quantum critical point, i.e. where correlations become long-ranged and full updating of the environment tensor becomes essential [16].

Here we generalize the simple update method to study the PESS wave function, by utilizing the HOSVD of tensors [11, 23]. We again take the kagome lattice to illustrate the method. Figure 5 shows graphical representations of the 3-PESS, the 5-PESS, and the 9-PESS, which are the three simplest available PESS wave functions on the kagome lattice. We stress again that each one takes into account all the correlations (or entanglement) among the  $N$  spins on the corresponding simplex, described by the entangled simplex tensor  $S$ . In the limit of large  $D$ , this simplex entanglement is treated rigorously. For simplicity, we describe only the 3-PESS in detail below. It is straightforward to extend the method to other PESS representations and to different lattices.

We write the Hamiltonian in the form

$$H = H_\Delta + H_\nabla, \quad (26)$$

where  $H_\Delta$  and  $H_\nabla$  are the Hamiltonians defined respectively on all upward- and downward-oriented triangular simplices. As shown in Fig. 5, the 3-PESS is defined on a honeycomb lattice formed by the simplex triangles. We assume the ground-state wave function to be translationally invariant within each sublattice formed by the “up” or “down” triangle simplices, and hence that the simplex tensors are the same on the same sublattice. The ground-state wave function may then be expressed as

$$|\Psi\rangle = \text{Tr}(\dots S_{a'b'c'}^\alpha A_{a'a}[\sigma_i] A_{b'b}[\sigma_j] A_{c'c}[\sigma_k] \dots) |\dots \sigma_i \sigma_j \sigma_k \dots\rangle, \quad (27)$$

where  $\alpha$  represents the vertex coordinates of the simplex honeycomb lattice and  $S^\alpha$  is the corresponding entangled simplex tensor. As in Sec. II, the physical basis states  $\{\sigma_i, \sigma_j, \dots\}$  are defined on the kagome lattice sites  $\{i, j, \dots\}$  and the Roman letters  $\{a, b, \dots\}$  denote the virtual bond states.

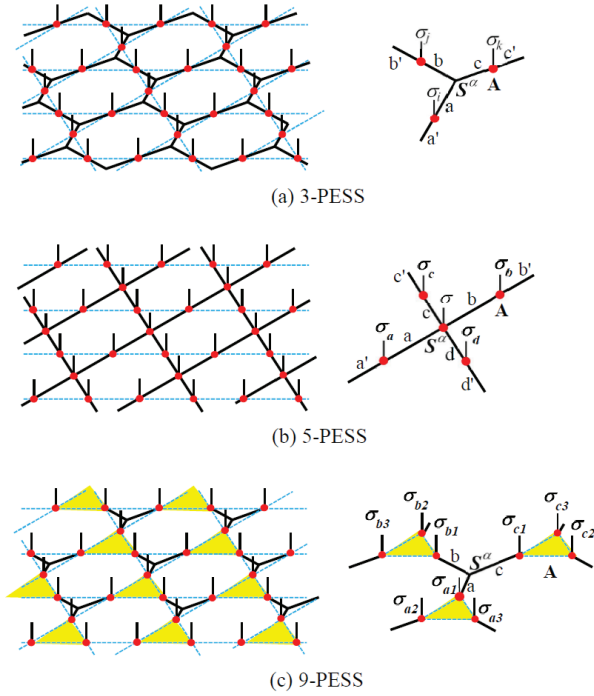


FIG. 5: (Color online) Graphical representations of a 3-PESS, 5-PESS, and 9-PESS on the kagome lattice (blue dashed lines). (a) The 3-PESS is defined on the decorated honeycomb lattice. The vertical dangling bonds represent the physical degrees of freedom  $\{\sigma_i, \dots\}$ .  $S^\alpha$  is the entangled three-index simplex tensor and  $A$  is a three-index tensor defined at each physical lattice site. (b) The 5-PESS is defined on the decorated square lattice. The entangled simplex tensor  $S^\alpha$  has five indices, one of which represents the physical basis states at the nodes of the square lattice while the other four represent the four virtual bond states connecting to the neighboring decorated sites; it takes into account all of the entanglement among these five spins. A tensor-network ansatz with the same structure as this 5-PESS has been used in Ref. [24] for studying the ground state of the  $SU(N)$  model on the kagome lattice. (c) The 9-PESS is defined by taking the three spins on each upward-oriented triangle as one effective site. The entangled simplex tensor  $S^\alpha$  has three indices and describes all of the entanglement among the nine spins it connects.

### A. HOSVD procedure

As in Sec. III, the ground-state wave function is determined by applying the imaginary-time evolution operator  $\exp(-\tau H)$  to an arbitrary initial state  $|\Psi_0\rangle$ , and in the limit  $\tau \rightarrow \infty$  the projected state  $\exp(-\tau H)|\Psi_0\rangle$  will converge to the ground state. This projection cannot be performed in a single step because the two terms in the Hamiltonian (26) do not commute with each other. To carry out the projection, we take a small value for  $\tau$  and apply the evolution operator to  $|\Psi_0\rangle$  iteratively over many steps. In the limit  $\tau \rightarrow 0$ , the evolution operator may be decomposed approximately into the product of

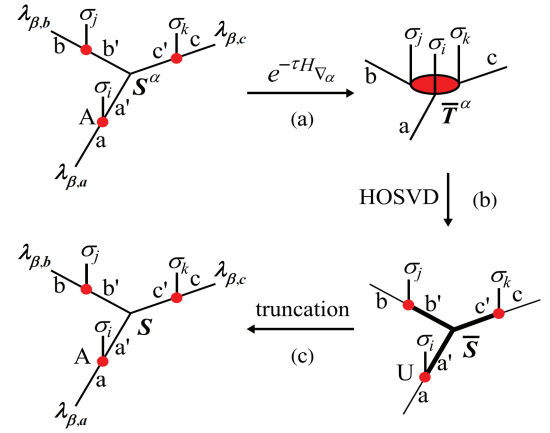


FIG. 6: (Color online) Flowchart for the simple update renormalization scheme for the wave function using HOSVD. The environment contribution around simplex  $\alpha$  is described by a singular bond vector  $\lambda_\beta$  on each bond connected with the environment;  $\lambda_\beta$  is an approximate measure of the entanglement on this bond. (a)  $\exp(-\tau H_{\nabla\alpha})$  acts on the tensors in a simplex to produce a new tensor  $\bar{T}^\alpha$  defined by Eq. (30). (b)  $\bar{T}$  is decomposed by HOSVD [Eq. (31)] into the product of a simplex tensor  $\bar{S}$  and three unitary matrices  $U$ . The dimensions of the thick and thin black bonds are respectively  $dD$  and  $D$ . (c) The thick bond dimension is truncated from  $dD$  to  $D$ , defining the renormalized  $S$  and  $A$  tensors.

two terms by the Trotter-Suzuki formula,

$$e^{-\tau H} = e^{-\tau H_\Delta} e^{-\tau H_\nabla} + \mathcal{O}(\tau^2). \quad (28)$$

Each projection is then performed in two steps, by applying  $\exp(-\tau H_\Delta)$  and  $\exp(-\tau H_\nabla)$  successively to the wave function.

We first consider the projection with  $H_\nabla$ . A schematic representation of this procedure is shown in Fig. 6. Because all of the separate terms in  $H_\nabla$  commute with each other, the action of the projection operator  $\exp(-\tau H_\nabla)$  on a wave function of the form specified by Eq. (27) can be expressed as a product of local evolution operators defined on each simplex (down triangle),

$$e^{-\tau H_\nabla} |\Psi_0\rangle = \text{Tr}(\dots T_{a\sigma_i, b\sigma_j, c\sigma_k}^{\alpha\nabla} S_{ade}^{\beta\Delta} \dots) |\dots \sigma_i \sigma_j \sigma_k \dots\rangle,$$

where  $T_{a\sigma_i, b\sigma_j, c\sigma_k}^{\alpha\nabla}$  is a  $dD \times dD \times dD$  tensor defined by

$$T_{a\sigma_i, b\sigma_j, c\sigma_k}^{\alpha\nabla} = \sum_{\sigma'_i \sigma'_j \sigma'_k a' b' c'} \langle \sigma_i \sigma_j \sigma_k | e^{-\tau H_{\nabla\alpha}} | \sigma'_i \sigma'_j \sigma'_k \rangle \times S_{a'b'c'}^{\alpha\nabla} A_{a'a}[\sigma'_i] A_{b'b}[\sigma'_j] A_{c'c}[\sigma'_k] \quad (29)$$

and  $S_{ade}^{\beta\Delta}$  represents the simplex tensors of the up triangles, which are renormalized in the next step of the projection (below). In Eq. (29),  $H_{\nabla\alpha}$  is the Hamiltonian for the simplex  $\alpha$  and the local projection operator couples the simplex tensor  $S^{\alpha\nabla}$  with the three neighboring  $A$  tensors. For notational simplicity, in the remainder

of this section the superscript  $\alpha$  refers to down triangles and  $\beta$  to up triangles.

The next step is HOSVD, to decompose the tensor  $T_{a\sigma_i, b\sigma_j, c\sigma_k}^\alpha$  into the product of a renormalized simplex tensor and three renormalized projection ( $A$ ) tensors. At this step one should also include the renormalization effect of the environment tensors surrounding  $T^\alpha$  [Fig. 6]. Here we adopt an approximate scheme to simulate the contribution of the environment tensors [8] by introducing a positive singular bond vector  $\lambda_\beta$  (or  $\lambda_\alpha$ ) of dimension  $D$  on each bond linking the  $S^\alpha$  (or  $S^\beta$ ) and  $A$  tensors. This singular bond vector may be determined iteratively by diagonalizing a density matrix  $W$ , which is defined below, and it measures the entanglement between the corresponding basis states on the two ends of the bond. This motivates the definition of an environment-renormalized  $T^\alpha$  tensor,

$$\bar{T}_{a\sigma_i, b\sigma_j, c\sigma_k}^\alpha = \lambda_{\beta, a} \lambda_{\beta, b} \lambda_{\beta, c} T_{a\sigma_i, b\sigma_j, c\sigma_k}^\alpha, \quad (30)$$

where the three bonds of  $T^\alpha$  are weighted by the corresponding singular bond vectors. These additional bond vectors are included to mimic the renormalization effect from the environment tensors in an effective entanglement mean-field approach, which avoids the (computationally expensive) full calculation of the tensor environment.

To truncate  $\bar{T}^\alpha$  into a tensor of lower rank, we use a HOSVD to decompose it according to

$$\bar{T}_{a\sigma_i, b\sigma_j, c\sigma_k}^\alpha = \sum_{a'b'c'} \bar{S}_{a'b'c'}^\alpha U_{a', a\sigma_i} U_{b', b\sigma_j} U_{c', c\sigma_k}, \quad (31)$$

where  $\bar{S}^\alpha$  is the core tensor of  $\bar{T}^\alpha$ , and satisfies two key properties for any given index. We illustrate these using the second index  $b$ :

(1) fully orthogonal:

$$\langle \bar{S}_{:,b,:}^\alpha | \bar{S}_{:,b',:}^\alpha \rangle = 0, \quad \text{if } b \neq b',$$

where  $\langle \bar{S}_{:,b,:}^\alpha | \bar{S}_{:,b',:}^\alpha \rangle$  is the inner product of the two subtensors.

(2) pseudodiagonal:

$$|\bar{S}_{:,b,:}^\alpha| \geq |\bar{S}_{:,b',:}^\alpha|, \quad \text{if } b < b',$$

where  $|\bar{S}_{:,b,:}^\alpha|$  is the norm of this subtensor, equal to the square root of the sum of squares of all elements. These norms play a role similar to the singular values of the matrix.

In Eq. (31),  $U$  is a unitary matrix of dimension  $dD \times dD$ , determined by diagonalizing the density matrix

$$\begin{aligned} W_{a\sigma_i, \underline{a\sigma_i}} &= \sum_{bc\sigma_j\sigma_k} \bar{T}_{a\sigma_i, b\sigma_j, c\sigma_k}^\alpha \bar{T}_{\underline{a\sigma_i}, b\sigma_j, c\sigma_k}^\alpha \\ &= \sum_{a'} U_{a', a\sigma_1} \lambda_{\alpha, a'}^2 U_{a', \underline{a\sigma_1}}, \end{aligned}$$

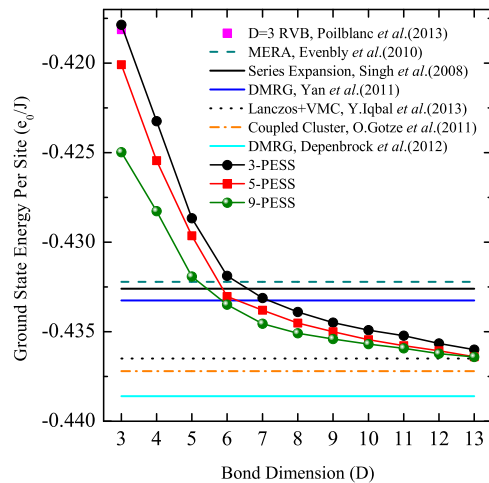


FIG. 7: (Color online) The dependence on bond dimension  $D$  of the ground-state energy of the  $S = 1/2$  kagome Heisenberg antiferromagnet obtained using 3-PESS, 5-PESS, and 9-PESS tensor-network representations. The upper bounds on the ground-state energy obtained by a PEPS RVB ansatz [40], MERA [31], series-expansion methods based on valence-bond crystal states [29, 30], DMRG [35], Lanczos exact diagonalization and VMC based on a gapless Dirac spin-liquid state [39], and a high-order coupled-cluster expansion [44], as well as the DMRG result obtained by extrapolation [36], are shown for comparison.

where  $\lambda_{\alpha, a'}^2$  are the eigenvalues of  $W$ , which measure the weights of the corresponding basis vectors  $U_{a'}$  in  $\bar{T}^\alpha$ . With the aid of the  $U$  matrices, we define the renormalized  $A$  tensor by

$$A_{a'a}[\sigma] = U_{a', a\sigma} \lambda_{\beta, a}^{-1},$$

where the dimension of the  $a'$  bond is truncated to  $D$ . Finally, by keeping the first  $D$  states for all three bond directions, we truncate  $\bar{S}^\alpha$  to a  $D \times D \times D$  tensor  $S^\alpha$ . This renormalized  $S^\alpha$  tensor defines the new entangled simplex tensor for its sublattice.

The projection with  $\exp(-\tau H_\Delta)$  is performed in the same way. By repeating this iteration procedure, an accurate ground-state wave function is obtained after sufficiently many steps. The truncation error in the tensors describing the ground-state wave function is reduced iteratively throughout this renormalization procedure, and the iteration can be terminated when the truncation error falls below a desired value.

## B. Ground-state energy for the spin-1/2 kagome antiferromagnet

We have applied the simple update scheme to the PESS representation of the spin-1/2 Heisenberg antiferromagnet on the kagome lattice. The ground state



of this frustrated spin system has long been thought to be an ideal candidate quantum spin liquid, a magnetic system with no spontaneous symmetry breaking but showing specific topological order [25]. This model has been studied by approximate approaches for several decades [26], with many proposals for the nature of the ground state. Early numerical calculations [27] suggested that the ground state of the model might be a valence-bond crystal, breaking the translational symmetry of the kagome lattice, and this state has also been supported by analytical arguments [28], by detailed cluster calculations [29, 30], by the multiscale entanglement renormalization ansatz (MERA) [31], and by variational Monte Carlo (VMC) studies [32]. By contrast, different analytical arguments [33] and extensive DMRG studies [34–36] have all found the ground state to be a spin liquid with a finite gap to triplet excitations; recent efforts to establish the topological properties of this state [36, 37] indicate that it is the  $Z_2$  spin liquid known from quantum dimer models. Other authors still have suggested [38, 39] that the ground state is a gapless, algebraic quantum spin liquid. We comment here that Poilblanc and coworkers [40–42] have recently proposed a PEPS-based trial wave function with resonating valence-bond (RVB) character specifically to study the  $Z_2$  spin-liquid phase. Their wave function, which they found to work very well for this model, is actually a 3-PESS with  $D = 3$ .

Before presenting our results, we discuss the calculation of ground-state expectation values using the PESS wave function. The calculation of the wave function, as detailed in Secs. III and IVA, is a fully variational procedure and is subject to a truncation error that can be made arbitrarily small by reducing  $\tau$ . To obtain an expectation value, we project the wave function onto an MPS basis and calculate the required quantities using the infinite time-evolving block-decimation method [6]. While this procedure is not variational, the error in this part of the calculation may be obtained by systematic variation of the bond dimension,  $D_{mps}$ , of the MPS basis. When more than 60 basis states are retained ( $D_{mps} > 60$ ), the truncation error due to the evaluation procedure is less than  $10^{-4}$  for all of the 3-PESS and 9-PESS results shown in Fig. 7; however, it is somewhat higher for the 5-PESS, where it varies up to a maximum of approximately  $2 \times 10^{-3}$  for  $D = 13$ , even with  $D_{mps} = 140$ . We discuss this topic in further detail below.

Our result for the ground-state energy per site,  $e_0$ , of the kagome Heisenberg antiferromagnet is shown in Fig. 7 as a function of the bond dimension  $D$ , for the 3-PESS, 5-PESS, and 9-PESS representations (Fig. 5). As expected, the ground-state energy falls with increasing  $D$ . In a gapped system, the ground state should converge exponentially with  $D$ . However, the energies we obtain have not yet reached the exponentially converged regime for any of the PESS representations, even for  $D = 13$ . For this reason, we do not attempt an extrapolation to the large- $D$  limit, because the results would be of limited meaning with the available data and may be sub-

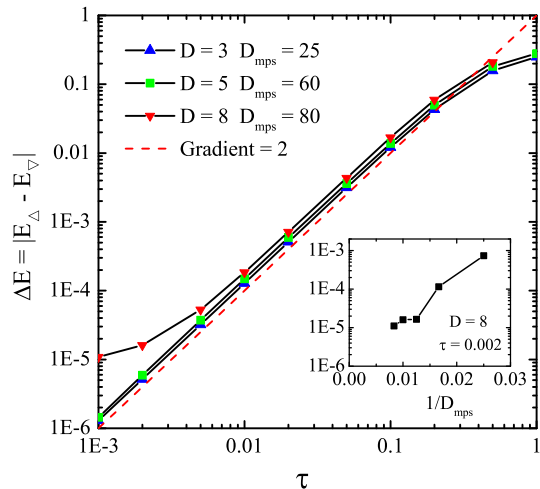


FIG. 8: (Color online) Energy difference between up and down triangles in the 3-PESS, shown for different bond dimensions  $D$  as a function of Trotter step size  $\tau$ . The dashed line shows the function  $\tau^2$ , indicating that the energy difference vanishes in the limit  $\tau \rightarrow 0$ . For higher values of  $D$ , calculations with higher values of  $D_{mps}$  are required for full convergence. Inset: the dependence of the energy difference on  $D_{mps}$  shows a rapid convergence to values  $D_{mps}$  of order  $D^2$ , followed by a slow convergence dictated by  $\tau$ .

ject to significant errors. We stress that our result is variational, hence representing an upper energy bound, and that this bound can clearly be lowered quite significantly by further increasing  $D$ . We remind the reader that our method is for a system infinite in size, with truncation effected through  $D$ , and thus our results set an upper bound for  $e_0$  in the infinite two-dimensional limit. This new bound is the value we obtain for the 9-PESS at  $D = 13$ ,  $e_0 = -0.4364(1)J$ .

In fact all three PESS values for the ground-state energy already lie lower than the energies of the proposed valence-bond-crystal states [29–31], and the best energy obtained by contractor renormalization [43], for  $D = 7$ . Larger values of  $D$  are required before the PESS values fall below the upper bound obtained by DMRG in Ref. [35]. While the trend is clearly visible in Fig. 7, we have not yet been able to reach values of  $D$  sufficiently large that our calculated ground-state energy falls below that obtained by the most sophisticated variational projector quantum Monte Carlo calculations for the gapless spin-liquid scenario ( $e_0 = -0.4365J$ ) [39], from the optimal extrapolated value in the most detailed high-order coupled-cluster approach ( $e_0 = -0.4372J$ ) [44], which favors a gapped spin liquid, or the approximate value estimated recently from DMRG calculations by Depenbrock *et al.*,  $e_0 = -0.4386(5)J$  [36]. This last estimate may not be a true upper bound for  $e_0$  because it was obtained by an extrapolation of DMRG results that continue to show a quite significant finite-size oscillation.

Regarding the qualitative properties of the ground state whose wave function we have deduced, we make a further important comment concerning its symmetry. The 3-PESS and 9-PESS break the symmetry between up and down triangles, while the 5-PESS breaks the three-fold rotational symmetry of the kagome lattice. We have studied the energy differences induced in this way, and illustrate their evolution with both Trotter step size  $\tau$  and MPS bond dimension  $D_{mps}$  in Fig. 8 for the example of the up-down asymmetry between triangles in the 3-PESS. This calculation also illustrates the nature of the truncation error in the MPS calculation of expectation values, where the effects of finite  $\tau$ ,  $D$ , and  $D_{mps}$  are interdependent. It is clear that the energy difference tends to zero, restoring the symmetry of the ground-state wave function, as  $\tau \rightarrow 0$  at fixed  $D$  and  $D_{mps}$ . This difference is in fact a direct measure of the truncation error in the wave function, which is fully controlled by  $\tau$ . The inset indicates that symmetry restoration is also approached in the asymptotic limit of large  $D_{mps}$ , where again it is limited by the value of  $\tau$ . Thus we can state with confidence that the lattice symmetries are preserved in the true ground state. We expect that physical quantities calculated from the PESS wave function, including single-site magnetizations and single-bond spin correlation functions, will show the same property of weak, symmetry-broken differences tending to a uniform value in the appropriate limits.

We remark again that our ground-state wave function is obtained on the basis of the simple update approximation. By adopting this procedure we have essentially sacrificed a precise accounting for the effects of the bond environment in exchange for the accuracy inherent in accessing larger values of the tensor dimension  $D$ . Such an approach underestimates the long-range correlation (entanglement) of the spins. To improve on this result, and to calculate the correlation functions with the maximum accuracy available within the PESS framework, one should perform a full-update calculation taking complete account of the bond environment. We leave this generally very time-consuming task for future study.

## V. SUMMARY

We have introduced the projected entangled simplex states (PESS) as a new class of tensor-network states embodying the entanglement of particles within a simplex. It is an exact tensor-network representation of the simplex solid states first introduced by Arovas [21]. We have demonstrated, using an  $SU(2)$  simplex solid state for  $S = 2$  spins on the kagome lattice, how to construct the PESS wave function and the parent Hamiltonian. The discussion can be generalized to  $SU(N)$  or other groups and to all lattice geometries.

PESS, together with projected entangled pair states (PEPS), form a comprehensive representation of tensor-network states that satisfy the area law of entanglement

entropy [20]. They arise naturally in the context of constructing trial wave functions for quantum systems on two- or higher-dimensional lattices. For a wide variety of systems, PESS provide an efficient representation of the exponential number of coefficients by a small number of parameters describing the low-energy physics of many-body quantum states arising from local interactions. As for PEPS, PESS correlation functions are short-ranged, and so results obtained with the PESS representation should converge exponentially with increasing bond dimension  $D$  for sufficiently large  $D$  in a gapped system. For a translationally invariant system, the PESS calculation is performed directly on an infinite lattice, bypassing completely the errors inherent in extrapolations from finite-size calculations.

PEPS and PESS are two types of trial wave function. In systems where the correlation between pairs of neighboring sites are strongest, such as an AKLT state, then PEPS are appropriate. If correlations among all the basis states in a simplex or a larger cluster become important, then the PESS representation is required. From our studies of the spin-1/2 kagome Heisenberg antiferromagnet, the failure of PEPS to converge, contrasted with the success of PESS, indicate that the effects of frustration in the kagome geometry are well accounted for by the entangled simplex tensor  $S_{abc}$ . An underlying reason for the success of the PESS wavefunction on the kagome lattice may be that it is defined on the decorated honeycomb lattice, which is geometrically unfrustrated. These observations suggest that the problem of geometrical frustration in other lattices can be similarly and approximately solved by finding a PESS representation whose local tensors form an unfrustrated lattice.

PESS are also superior to PEPS in that the orders of the local tensors are reduced in certain lattices. A particular example is the triangular lattice, where in the PEPS representation the total number of tensor elements is  $dD^6$ , while in a PESS representation (Fig. 2) the two tensors contain only  $D^3$  and  $dD^3$  elements. Still, a rigorous evaluation of all local tensors in a PESS representation, including the corresponding expectation values, requires a trace over all indices. This is an exponentially hard problem and one not directly tractable for large lattice systems, but approximate contraction schemes have been devised to overcome this limitation. In the calculation of expectation values, there is little difference between PEPS and PESS; the methods developed for evaluating expectation values based on PEPS can be extended straightforwardly to PESS.

To determine the PESS wave function, we have introduced a simple but efficient update approach based on HOSVD. This is basically an entanglement mean-field approach, which leads to a scalable variational method for finding the local tensors. We have applied this method to the spin-1/2 Heisenberg antiferromagnet on the kagome lattice and obtained an excellent estimate of the ground-state energy,  $e_0 = -0.4364(1)J$  (from the 9-PESS with  $D = 13$ ). This very promising result can be further im-

proved by enlarging the order and the bond dimension of the local tensors within the simple update scheme, or more rigorously by a full update of the bond environment tensors. This latter step will allow one to evaluate accurately the correlation functions and the entanglement spectra. Efforts in this direction should help to make a definitive identification of the topological phase in the ground state of the kagome Heisenberg model.

The PESS representation can be readily extended to other lattices and other models. It provides a significant advantage in studying the ground-state properties of quantum lattice models on the triangular (Fig. 2), square (Fig. 3), and other lattices, because the order of the local tensors on these lattices is much smaller than for the corresponding PEPS. In particular, we believe that the PESS representation shown in Fig. 3(b) offers many advantages over PEPS for studying the  $J_1$ – $J_2$  an-

tiferromagnetic Heisenberg model on the square lattice [45–47]. Finally, by proceeding as for the development of fermionic PEPS [48–51], the PESS framework can also be extended to include fermionic degrees of freedom.

### Acknowledgments

We thank P. Corboz for valuable discussions, including those leading us to correct Fig. 7, and W. Li, D. Poilblanc, and H. H. Tu for helpful comments. This work was supported by the National Natural Science Foundation of China (Grant Nos. 10934008, 10874215, and 11174365) and by the National Basic Research Program of China (Grant Nos. 2012CB921704 and 2011CB309703).

- 
- [1] H. Niggemann, A. Klumper, and J. Zittartz, *Quantum phase transition in spin-3/2 systems on the hexagonal lattice - optimum ground state approach*, Z. Phys. B **104**, 103 (1997).
- [2] G. Sierra and M. Martin-Delgado, *Proceedings of the Workshop on the Exact Renormalization Group*, (World Scientific, Singapore, 1999).
- [3] T. Nishino, Y. Hieida, K. Okunishi, N. Maeshima, Y. Akutsu, and A. Gendiar, *Two-Dimensional Tensor Product Variational Formulation*, Prog. Theor. Phys. **105**, 409 (2001).
- [4] F. Verstraete and J. I. Cirac, *Renormalization algorithms for Quantum-Many Body Systems in two and higher dimensions*, unpublished (cond-mat/0407066).
- [5] G. Vidal, *Efficient Classical Simulation of Slightly Entangled Quantum Computations*, Phys. Rev. Lett. **91**, 147902 (2003); *ibid.* **93**, 040502 (2004).
- [6] G. Vidal, *Classical Simulation of Infinite-Size Quantum Lattice Systems in One Spatial Dimension*, Phys. Rev. Lett. **98**, 070201 (2007).
- [7] M. Levin and C. P. Nave, *Tensor Renormalization Group Approach to Two-Dimensional Classical Lattice Models*, Phys. Rev. Lett. **99**, 120601 (2007).
- [8] H. C. Jiang, Z. Y. Weng, and T. Xiang, *Accurate Determination of Tensor Network State of Quantum Lattice Models in Two Dimensions*, Phys. Rev. Lett. **101**, 090603 (2008).
- [9] Z. Y. Xie, H. C. Jiang, Q. N. Chen, Z. Y. Weng, and T. Xiang, *Second Renormalization of Tensor-Network States*, Phys. Rev. Lett. **103**, 160601 (2009).
- [10] H. H. Zhao, Z. Y. Xie, Q. N. Chen, Z. C. Wei, J. W. Cai, and T. Xiang, *Renormalization of tensor-network states*, Phys. Rev. B **81**, 174411 (2010).
- [11] Z. Y. Xie, J. Chen, M. P. Qin, J. W. Zhu, L. P. Yang, and T. Xiang, *Coarse-graining renormalization by higher-order singular value decomposition*, Phys. Rev. B **86**, 045139 (2012).
- [12] R. Orus, *A Practical Introduction to Tensor Networks: Matrix Product States and Projected Entangled Pair States*, unpublished (arXiv:1306.2164), and references therein.
- [13] Q. N. Chen, M. P. Qin, J. Chen, Z. C. Wei, H. H. Zhao, B. Normand, and T. Xiang, *Partial Order and Finite-Temperature Phase Transitions in Potts Models on Irregular Lattices*, Phys. Rev. Lett. **107**, 165701 (2011).
- [14] Z. C. Gu, M. Levin, and X. G. Wen, *Tensor-entanglement renormalization group approach as a unified method for symmetry breaking and topological phase transitions*, Phys. Rev. B **78**, 205116 (2008).
- [15] J. Jordan, R. Orus, G. Vidal, F. Verstraete, and J. I. Cirac, *Classical Simulation of Infinite-Size Quantum Lattice Systems in Two Spatial Dimensions*, Phys. Rev. Lett. **101**, 250602 (2008).
- [16] W. Li, J. von Delft, and T. Xiang, *Efficient simulation of infinite tree tensor network states on the Bethe lattice*, Phys. Rev. B **86**, 195137 (2012).
- [17] S. Östlund and S. Rommer, *Thermodynamic Limit of Density Matrix Renormalization*, Phys. Rev. Lett. **75**, 3537 (1995).
- [18] S. R. White, *Density matrix formulation for quantum renormalization groups*, Phys. Rev. Lett. **69**, 2863 (1992).
- [19] I. Affleck, T. Kennedy, E. H. Lieb, and H. Tasaki, *Rigorous results on valence-bond ground states in antiferromagnets*, Phys. Rev. Lett. **59**, 799 (1987); *Valence-bond ground states in isotropic quantum antiferromagnets*, Commun. Math. Phys. **115**, 477 (1988).
- [20] J. Eisert, M. Cramer, and M. B. Plenio, *Colloquium: Area laws for the entanglement entropy*, Rev. Mod. Phys. **82**, 277 (2010).
- [21] D. P. Arovas, *Simplex solid states of  $SU(N)$  quantum antiferromagnets*, Phys. Rev. B **77**, 104404 (2008).
- [22] H. H. Tu, private communication.
- [23] L. de Lathauwer, B. de Moor, and J. Vandewalle, *A Multilinear Singular Value Decomposition*, SIAM J. Matrix Anal. Appl. **21**, 1253 (2000).
- [24] P. Corboz, K. Penc, F. Mila, and A. M. Läuchli, *Simplex solids in  $SU(N)$  Heisenberg models on the kagome and checkerboard lattices*, Phys. Rev. B **86**, 041106 (2012).
- [25] L. Balents, *Spin liquids in frustrated magnets*, Nature **464**, 199 (2010).
- [26] V. Elser, *Nuclear antiferromagnetism in a registered  $^3\text{He}$  solid*, Phys. Rev. Lett. **62**, 2405 (1989).

- [27] J. B. Marston and C. Zeng, *Spin-Peierls and spin-liquid phases of kagome quantum antiferromagnets*, J. Appl. Phys. **69**, 5962 (1991).
- [28] P. Nikolic and T. Senthil, *Physics of low-energy singlet states of the kagome lattice quantum Heisenberg antiferromagnet*, Phys. Rev. B **68**, 214415 (2003).
- [29] R. R. P. Singh and D. A. Huse, *Ground state of the spin-1/2 kagome-lattice Heisenberg antiferromagnet*, Phys. Rev. B **76**, 180407 (2007).
- [30] R. R. P. Singh and D. A. Huse, *Triplet and singlet excitations in the valence bond crystal phase of the kagome-lattice Heisenberg model*, Phys. Rev. B **77**, 144415 (2008).
- [31] G. Evenbly and G. Vidal, *Frustrated Antiferromagnets with Entanglement Renormalization: Ground State of the Spin-1/2 Heisenberg Model on a Kagome Lattice*, Phys. Rev. Lett. **104**, 187203 (2010).
- [32] Y. Iqbal, F. Becca, and D. Poilblanc, *Valence-bond crystal in the extended kagome spin-1/2 quantum Heisenberg antiferromagnet: a variational Monte Carlo approach*, Phys. Rev. B **83**, 100404 (2011).
- [33] S. Sachdev, *Kagome- and triangular-lattice Heisenberg antiferromagnets: ordering from quantum fluctuations and quantum-disordered ground states with unconfined bosonic spinons*, Phys. Rev. B **45**, 12377 (1992).
- [34] H. C. Jiang, Z. Y. Weng, and D. N. Sheng, *Density Matrix Renormalization Group Numerical Study of the Kagome Antiferromagnet*, Phys. Rev. Lett. **101**, 117203 (2008).
- [35] S. Yan, D. A. Huse, and S. R. White, *Spin-Liquid Ground State of the  $S = 1/2$  Kagome Heisenberg Antiferromagnet*, Science **332**, 1173 (2011).
- [36] S. Depenbrock, I. P. McCulloch, and U. Schollwöck, *Nature of the Spin-Liquid Ground State of the  $S = 1/2$  Heisenberg Model on the Kagome Lattice*, Phys. Rev. Lett. **109**, 067201 (2012).
- [37] H. C. Jiang, Z. H. Wang, and L. Balents, *Identifying topological order by entanglement entropy*, Nature Phys. **8**, 902 (2012).
- [38] Y. Ran, M. Hermele, P. A. Lee, and X. G. Wen, *Projected-Wave-Function Study of the Spin-1/2 Heisenberg Model on the Kagome Lattice*, Phys. Rev. Lett. **98**, 117205 (2007).
- [39] Y. Iqbal, F. Becca, S. Sorella, and D. Poilblanc, *Gapless spin-liquid phase in the kagome spin-1/2 Heisenberg antiferromagnet*, Phys. Rev. B **87**, 060405 (2013).
- [40] D. Poilblanc, N. Schuch, D. Perez-Garcia, and J. I. Cirac, *Topological and entanglement properties of resonating valence bond wave functions*, Phys. Rev. B **86**, 014404 (2012).
- [41] N. Schuch, D. Poilblanc, J. I. Cirac, and D. Perez-Garcia, *Resonating valence bond states in the PEPS formalism*, Phys. Rev. B **86**, 115108 (2012).
- [42] D. Poilblanc and N. Schuch, *Simplex  $Z_2$  spin liquids on the kagome lattice with projected entangled pair states: spinon and vison coherence lengths, topological entropy, and gapless edge modes*, Phys. Rev. B **87**, 140407 (2013).
- [43] S. Capponi, V. R. Chandra, A. Auerbach, and M. Weinstein,  *$p_6$  chiral resonating valence bonds in the kagome antiferromagnet*, Phys. Rev. B **87**, 161118 (2013).
- [44] O. Götze, D. J. J. Farnell, R. F. Bishop, P. H. Y. Li, and J. Richter, *Heisenberg antiferromagnet on the kagome lattice with arbitrary spin: a higher-order coupled cluster treatment*, Phys. Rev. B **84**, 224428 (2011).
- [45] P. Chandra and B. Douçot, *Possible spin-liquid state at large  $S$  for the frustrated square Heisenberg lattice*, Phys. Rev. B **38**, 9335 (1988).
- [46] R. Melzi, P. Carretta, A. Lascialfari, M. Mrambrini, M. Troyer, P. Millet, and F. Mila,  *$Li_2VO(Si,Ge)O_4$ , a Prototype of a Two-Dimensional Frustrated Quantum Heisenberg Antiferromagnet*, Phys. Rev. Lett. **85**, 1318 (2000).
- [47] H. C. Jiang, H. Yao, and L. Balents, *Spin liquid ground state of the spin-1/2 square  $J_1$ - $J_2$  Heisenberg model*, Phys. Rev. B **86**, 024424 (2012).
- [48] P. Corboz, G. Evenbly, F. Verstraete, and G. Vidal, *Simulation of interacting fermions with entanglement renormalization*, Phys. Rev. A **81**, 010303 (2010).
- [49] C. V. Kraus, N. Schuch, F. Verstraete, and J. I. Cirac, *Fermionic projected entangled pair states*, Phys. Rev. A **81**, 052338 (2010).
- [50] Q. Q. Shi, S. H. Li, J. H. Zhao, and H. Q. Zhou, *Graded Projected Entangled-Pair State Representations and An Algorithm for Translationally Invariant Strongly Correlated Electronic Systems on Infinite-Size Lattices in Two Spatial Dimensions*, unpublished (arXiv:0907.5520).
- [51] Z. C. Gu, F. Verstraete, and X. G. Wen, *Grassmann tensor network states and its renormalization for strongly correlated fermionic and bosonic states*, unpublished (arXiv:1004.2563).